IEEE Access
Multidisciplinary | Rapid Review | Open Access Journal

Received July 31, 2019, accepted August 9, 2019, date of publication August 21, 2019, date of current version September 4, 2019.

Digital Object Identifier 10.1109/ACCESS.2019.2936600

RSS-AOA-Based Localization via Mixed Semi-Definite and Second-Order Cone Relaxation in 3-D Wireless Sensor Networks

QINKE QI[1], YOUMING LI[1], YONGQING WU[2], YONG WANG[1], YIN YUE[1], AND XUPENG WANG[1]

[1]Faculty of Electrical Engineering and Computer Science, Ningbo University, Ningbo 315211, China
[2]Institute of Acoustics, Chinese Academy of Sciences, Beijing 100190, China

Corresponding author: Youming Li (liyouming@nbu.edu.cn)

This work was supported in part by the National Natural Science Foundation of China under Grant 61571250 and Grant 61531018, in part by the Zhejiang Natural Science Foundation under Grant LY18F010010, and in part by the K. C. Wong Magna Fund of Ningbo University.

ABSTRACT In this paper, the target node localization problems based on hybrid RSS-AOA measurements in both noncooperative and cooperative three-dimensional (3-D) wireless sensor networks (WSNs) are discussed. By using novel error approximate expressions for both received signal strength (RSS) and angle-of-arrival (AOA) measurement models, new estimators based on the least squares (LS) criterion are proposed. These estimators can be transformed into mixed semi-definite programming (SDP) and second-order cone programming (SOCP) problems by applying convex relaxation techniques. In addition, the closed-form Cramer-Rao lower bound (CRLB) of the estimator on hybrid measurements in cooperative WSNs is also derived. Theoretical analysis and simulation results show that the Root Mean Square Error (RMSE) of the proposed hybrid RSS-AOA estimators is lower than that of the discussed estimators in both noncooperative and cooperative cases.

INDEX TERMS Received signal strength (RSS), angle-of-arrival (AOA), mixed semi-definite and second-order cone programming (SD/SOCP), wireless localization.

I. INTRODUCTION

Wireless sensor network is a distributed sensor network, which is generally composed of a large number of sensors. These sensors are distributed throughout the surveillance area to collaboratively sense, acquire, process, and transmit the perceived object information. In order to maintain low implementation costs, only a small number of sensors called anchor nodes are equipped with global positioning system (GPS) devices, other sensors called target nodes collect the location information of known anchor nodes and determine their locations by some localization schemes [1], [2]. In practical applications, the data collected is meaningless if the corresponding location information is unavailable. Therefore, how to estimate the target node locations is one of the key technologies in WSNs.

Localization schemes rely on different types of measurements. These measurements mainly include time-of-arrival (TOA) [3], [4], time-difference-of-arrival (TDOA) [5], [6], received signal strength (RSS) [7]–[12], and angle-of-arrival (AOA) [13], [14].

Target localization estimators based on a single kind of measurement have two main advantages due to their low complexity and cost [15], however, there exists great room for the estimation accuracy improvement, hybrid processing from the combined measurement systems has been proposed to improve the performance.

In [16], a target node localization problem based on RSS measurements was addressed by semi-definite relaxation techniques. In [17], by applying the unscented transformation (UT), the authors transformed the RSS-based target node localization problem into a weighted least squares problem (WLS), which can be solved by the bisection method. However, the methods mentioned above provide low estimation accuracy. To reduce the localization error, hybrid systems that use distance and angle measurements were presented in [18], where a linear least squares (LLS) estimator and an optimization-based estimator were proposed to estimate

The associate editor coordinating the review of this article and approving it for publication was Thanh Ngoc Dinh.

the location of the target node. These methods proposed in [16]–[18] were derived only in noncooperative WSNs. In general, the noncooperative localization method has two disadvantages: 1) only one target node can be identified at a time, and 2) only the information transmitted by anchor nodes within the communication range can be utilized, which limits the application of algorithms in large-scale WSNs. In cooperative approaches, each sensor is required more power transmission and has a great dependence on the network structure [2]. However, cooperative approaches can determine multiple target nodes simultaneously, therefore, attract more attention recently. Note that cooperative localization is a challenging problem, because the measurements between the target nodes are used for location estimation [19]. In [20], the RSS-based cooperative target localization estimator was proposed, which can only provide a good initial point and further improvement can be achieved by using the maximum likelihood (ML) method. In [21], the RSS-based cooperative localization method was derived which employs relative error estimation, and the method has remarkable performance. The method proposed in [13] is based on hybrid AOA-TDOA measurements, and a new benchmark defined in this method can be used to predict the threshold effect, simulation results demonstrate the exceptional performance of the estimator, but it requires a very complex process of time synchronization, which is a costly task. In [22], the authors addressed the target localization problem based on hybrid RSS-AOA measurements, which does not require a time synchronization process, and the RMSE of the estimator is much lower than that of the RSS-based estimator [23], however, the method ignores the weights of the noise terms, thus the performance still has room for improvement.

In this paper, we investigate the RSS-AOA based target localization problems in both noncooperative and cooperative 3-D WSNs. New estimators based on the LS criterion are derived for noncooperative and cooperative scenarios, then, by applying appropriate semi-definite relaxation techniques and second-order cone relaxation techniques, the estimators can be transformed into corresponding convex problems, respectively. Compared with AOA-TDOA based estimators, the proposed estimator in cooperative WSNs reduces the implementation costs and is suitable for large-scale networks. Furthermore, the proposed estimator significantly outperforms the RSS-based estimators.

The contributions of this paper are summarized as follows

1) We formulate novel estimators via the first-order Taylor expansion which tightly approximate the maximum-likelihood estimators for both noncooperative and cooperative cases.

2) We use convex relaxation techniques to transform the developed estimators into mixed SD/SOCP problems.

3) We derive the closed-form CRLB of the estimator on hybrid measurements in cooperative WSNs.

II. NONCOOPERATIVE LOCALIZATION

In this section, we discuss the target localization problem in 3-D noncooperative scenarios. We consider a WSN which consists of N anchor nodes and one target node, and the locations of the anchor nodes, denoted as $\boldsymbol{a}_1, \boldsymbol{a}_2, \ldots, \boldsymbol{a}_N \in \mathbb{R}^3$, are known, while the location of the target node, denoted as $\boldsymbol{x} \in \mathbb{R}^3$, is unknown.

For ease of understanding, the link between the target node and the ith anchor node in a noncooperative scenario is shown in Fig. 1.

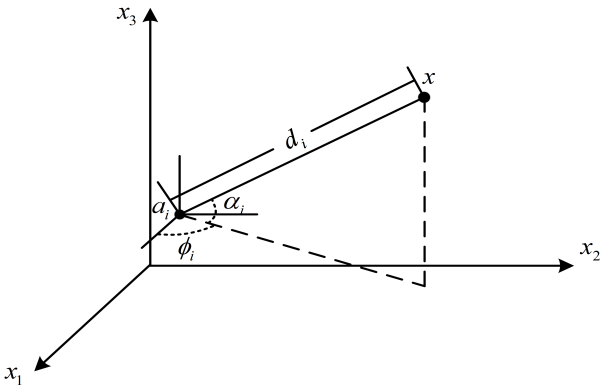

FIGURE 1. The link between the target node and the *i*th anchor node in a noncooperative scenario.

The RSS measurement model can be denoted by [22], [24], [25]

$$L_i = L_0 + 10\gamma \log_{10}\left(\frac{\|\boldsymbol{x}-\boldsymbol{a}_i\|}{d_0}\right) + n_i, \quad i = 1, \ldots, N \tag{1}$$

where L_0 denotes the reference path loss value at the reference distance d_0, γ denotes the path loss exponent (PLE), L_i denotes the path loss from the target node to the ith anchor node, and n_i represents the log-normal shadowing term, following the zero-mean Gaussian distribution with variance $\sigma_{n_i}^2$, *i.e.*, $n_i \sim \mathcal{N}(0, \sigma_{n_i}^2)$.

For ease of expression, we shall denote the unknown target node coordinates as $\boldsymbol{x} = [x_1, x_2, x_3]^T$ and the known coordinates of the ith anchor node as $\boldsymbol{a}_i = [a_{i1}, a_{i2}, a_{i3}]^T$, the azimuth angle measurement ϕ_i and elevation angle measurement α_i are related to the locations of the target node and the ith anchor node, modeled as [13], [18]

$$\phi_i = \arctan\left(\frac{x_2 - a_{i2}}{x_1 - a_{i1}}\right) + m_i, \quad i = 1, \ldots, N \tag{2}$$

$$\alpha_i = \arccos\left(\frac{x_3 - a_{i3}}{\|\boldsymbol{x} - \boldsymbol{a}_i\|}\right) + v_i, \quad i = 1, \ldots, N \tag{3}$$

where m_i and v_i are, respectively, the zero-mean Gaussian noises with variances of $\sigma_{m_i}^2$ and $\sigma_{v_i}^2$, modeled as $m_i \sim \mathcal{N}(0, \sigma_{m_i}^2)$, $v_i \sim \mathcal{N}(0, \sigma_{v_i}^2)$.

Equipped with additional hardware, the unknown target node can send calibration information to the anchor nodes,

which can be used to estimate the transmit power (reference path loss value) [2], [23]. So we assume the transmit power is known in this paper.

Swapping the positions of variables L_0 and L_i in equation (1), dividing both sides by 10γ, and then taking the power of 10, we obtain

$$10^{\frac{-L_i}{10\gamma}}\|\boldsymbol{x}-\boldsymbol{a}_i\|=10^{\frac{-L_0}{10\gamma}}d_0 10^{-\frac{n_i}{10\gamma}},\quad i=1,\ldots,N \tag{4}$$

The right side of equation (4) in high signal to noise ratio can be approximated by applying the first-order Taylor expansion as follows

$$10^{-\frac{n_i}{10\gamma}}\approx 1-\frac{\ln(10)}{10\gamma}n_i,\ i=1,\ldots,N \tag{5}$$

Substituting (5) into (4), we have

$$\lambda_i\|\boldsymbol{x}-\boldsymbol{a}_i\|\approx\mu d_0-\mu d_0\frac{\ln(10)}{10\gamma}n_i,\quad i=1,\ldots,N \tag{6}$$

where $\lambda_i=10^{\frac{-L_i}{10\gamma}}$, $\mu=10^{\frac{-L_0}{10\gamma}}$.

Moving the second item on the right side of equation (6) to the left side, squaring both sides and omitting the second-order noise term, we have

$$n_i\approx\frac{\beta^{-1}(\mu^2d_0^2-\lambda_i^2\|\boldsymbol{x}-\boldsymbol{a}_i\|^2)}{2\lambda_i\mu\|\boldsymbol{x}-\boldsymbol{a}_i\|},\quad i=1,\ldots,N \tag{7}$$

where $\beta=d_0\frac{\ln(10)}{10\gamma}$.

Similarly, equation (2) can be approximately expressed as

$$\xi_i\approx\boldsymbol{c}_i^T(\boldsymbol{x}-\boldsymbol{a}_i),\quad i=1,\ldots,N \tag{8}$$

where $\boldsymbol{c}_i=[-\sin\phi_i,\cos\phi_i,0]^T$, ξ_i refers to a weighted noise term, *i.e.*, $\xi_i=(\cos\phi_i(x_1-a_{i1})+\sin\phi_i(x_2-a_{i2}))m_i$.

Moving v_i to the left side of equation (3), taking cosine on both sides, and then applying the first-order Taylor expansion, we have

$$v_i\approx\frac{\boldsymbol{k}^T(\boldsymbol{x}-\boldsymbol{a}_i)-\cos\alpha_i\|\boldsymbol{x}-\boldsymbol{a}_i\|}{\sin\alpha_i\|\boldsymbol{x}-\boldsymbol{a}_i\|},\quad i=1,\ldots,N \tag{9}$$

where $\boldsymbol{k}=[0,0,1]^T$.

According to LS criterion, the objective function can be obtained as follows

$$\begin{aligned}\min_{\boldsymbol{x}}\ &\sum_{i=1}^{N}\left[\frac{\beta^{-1}(\mu^2d_0^2-\lambda_i^2\|\boldsymbol{x}-\boldsymbol{a}_i\|^2)}{2\lambda_i\mu\|\boldsymbol{x}-\boldsymbol{a}_i\|}\right]^2\\&+\sum_{i=1}^{N}\left[\boldsymbol{c}_i^T(\boldsymbol{x}-\boldsymbol{a}_i)\right]^2\\&+\sum_{i=1}^{N}\left[\frac{\boldsymbol{k}^T(\boldsymbol{x}-\boldsymbol{a}_i)-\cos\alpha_i\|\boldsymbol{x}-\boldsymbol{a}_i\|}{\sin\alpha_i\|\boldsymbol{x}-\boldsymbol{a}_i\|}\right]^2\end{aligned} \tag{10}$$

Introducing auxiliary variables f_i, we have

$$\begin{aligned}\min_{\boldsymbol{x}\boldsymbol{f}}\ &\sum_{i=1}^{N}\left[\frac{\beta^{-1}(\mu^2d_0^2-\lambda_i^2\|\boldsymbol{x}-\boldsymbol{a}_i\|^2)}{2\lambda_i\mu\|\boldsymbol{x}-\boldsymbol{a}_i\|}\right]^2+\|\boldsymbol{f}\|^2\\&+\sum_{i=1}^{N}\left[\frac{\boldsymbol{k}^T(\boldsymbol{x}-\boldsymbol{a}_i)-\cos\alpha_i\|\boldsymbol{x}-\boldsymbol{a}_i\|}{\sin\alpha_i\|\boldsymbol{x}-\boldsymbol{a}_i\|}\right]^2\\\text{s.t. }&f_i=\boldsymbol{c}_i^T(\boldsymbol{x}-\boldsymbol{a}_i),\quad i=1,\ldots,N\end{aligned} \tag{11}$$

Problem (11) can be expressed equivalently in the epigraph form

$$\begin{aligned}\min_{\boldsymbol{x},\boldsymbol{e},\boldsymbol{f},\boldsymbol{g},t}\ &\sum_{i=1}^{N}e_i+t+\sum_{i=1}^{N}g_i\\\text{s.t. }&\left[\frac{\beta^{-1}(\mu^2d_0^2-\lambda_i^2\|\boldsymbol{x}-\boldsymbol{a}_i\|^2)}{2\lambda_i\mu\|\boldsymbol{x}-\boldsymbol{a}_i\|}\right]^2\le e_i\\&\left[\frac{\boldsymbol{k}^T(\boldsymbol{x}-\boldsymbol{a}_i)-\cos\alpha_i\|\boldsymbol{x}-\boldsymbol{a}_i\|}{\sin\alpha_i\|\boldsymbol{x}-\boldsymbol{a}_i\|}\right]^2\le g_i\\&f_i=\boldsymbol{c}_i^T(\boldsymbol{x}-\boldsymbol{a}_i),\quad i=1,\ldots,N\\&\|\boldsymbol{f}\|^2\le t\end{aligned} \tag{12}$$

Inequality constraints in (12) can be converted to second-order cones

$$\begin{aligned}\min_{\boldsymbol{x},\boldsymbol{e},\boldsymbol{f},\boldsymbol{g},t}\ &\sum_{i=1}^{N}e_i+t+\sum_{i=1}^{N}g_i\\\text{s.t. }&\left\|\begin{bmatrix}\beta^{-1}(\mu^2d_0^2-\lambda_i^2\|\boldsymbol{x}-\boldsymbol{a}_i\|^2)\\\lambda_i^2\mu^2\|\boldsymbol{x}-\boldsymbol{a}_i\|^2-e_i\end{bmatrix}\right\|\\&\le\lambda_i^2\mu^2\|\boldsymbol{x}-\boldsymbol{a}_i\|^2+e_i\\&\left\|\begin{bmatrix}2(\boldsymbol{k}^T(\boldsymbol{x}-\boldsymbol{a}_i)-\cos\alpha_i\|\boldsymbol{x}-\boldsymbol{a}_i\|)\\\sin^2\alpha_i\|\boldsymbol{x}-\boldsymbol{a}_i\|^2-g_i\end{bmatrix}\right\|\\&\le\sin^2\alpha_i\|\boldsymbol{x}-\boldsymbol{a}_i\|^2+g_i\\&f_i=\boldsymbol{c}_i^T(\boldsymbol{x}-\boldsymbol{a}_i),\quad i=1,\ldots,N\\&\left\|\begin{bmatrix}\boldsymbol{f}\\t-1/4\end{bmatrix}\right\|\le t+1/4\end{aligned} \tag{13}$$

We introduce auxiliary variables $h_i=\|\boldsymbol{x}-\boldsymbol{a}_i\|^2$, $r_i=\|\boldsymbol{x}-\boldsymbol{a}_i\|$, then problem (13) can be rewritten as the following form

$$\begin{aligned}\min_{\substack{\boldsymbol{x},\boldsymbol{e},\boldsymbol{f},\boldsymbol{g}\\\boldsymbol{h},\boldsymbol{r},t}}\ &\sum_{i=1}^{N}e_i+t+\sum_{i=1}^{N}g_i\\\text{s.t. }&\left\|\begin{bmatrix}\beta^{-1}(\mu^2d_0^2-\lambda_i^2h_i)\\\lambda_i^2\mu^2h_i-e_i\end{bmatrix}\right\|\le\lambda_i^2\mu^2\,h_i+e_i\\&h_i=\begin{bmatrix}\boldsymbol{a}_i^T&-1\end{bmatrix}\begin{bmatrix}\boldsymbol{I}_3&\boldsymbol{x}\\\boldsymbol{x}^T&\boldsymbol{x}^T\boldsymbol{x}\end{bmatrix}\begin{bmatrix}\boldsymbol{a}_i\\-1\end{bmatrix}\\&\left\|\begin{bmatrix}2(\boldsymbol{k}^T(\boldsymbol{x}-\boldsymbol{a}_i)-\cos\alpha_ir_i)\\\sin^2\alpha_ih_i-g_i\end{bmatrix}\right\|\le\sin^2\alpha_ih_i+g_i\\&r_i=\|\boldsymbol{x}-\boldsymbol{a}_i\|\\&f_i=\boldsymbol{c}_i^T(\boldsymbol{x}-\boldsymbol{a}_i),\quad i=1,\ldots,N\\&\left\|\begin{bmatrix}\boldsymbol{f}\\t-1/4\end{bmatrix}\right\|\le t+1/4\end{aligned} \tag{14}$$

In order to turn the problem (14) into a convex problem, we define $z=\boldsymbol{x}^T\boldsymbol{x}$, then relax $z=\boldsymbol{x}^T\boldsymbol{x}$ and $r_i=\|\boldsymbol{x}-\boldsymbol{a}_i\|$ to $z\ge\boldsymbol{x}^T\boldsymbol{x}$ and $r_i\ge\|\boldsymbol{x}-\boldsymbol{a}_i\|$ respectively [26], resulting in the

following convex estimator

$$\begin{aligned}
&\min_{\substack{\boldsymbol{x},\boldsymbol{e},\boldsymbol{f},\boldsymbol{g}\\ \boldsymbol{h},\boldsymbol{r},t,z}} \sum_{i=1}^{N} e_i + t + \sum_{i=1}^{N} g_i \\
&\text{s.t.} \left\| \begin{bmatrix} \beta^{-1}(\mu^2 d_0^2 - \lambda_i^2 h_i) \\ \lambda_i^2 \mu^2 h_i - e_i \end{bmatrix} \right\| \le \lambda_i^2 \mu^2 \, h_i + e_i \\
&\quad h_i = \begin{bmatrix} \boldsymbol{a}_i^T & -1 \end{bmatrix} \begin{bmatrix} \boldsymbol{I}_3 & \boldsymbol{x} \\ \boldsymbol{x}^T & z \end{bmatrix} \begin{bmatrix} \boldsymbol{a}_i \\ -1 \end{bmatrix} \\
&\quad \left\| \begin{bmatrix} 2(\boldsymbol{k}^T(\boldsymbol{x} - \boldsymbol{a}_i) - \cos\alpha_i r_i) \\ \sin^2\alpha_i h_i - g_i \end{bmatrix} \right\| \le \sin^2\alpha_i h_i + g_i \\
&\quad r_i \ge \|\boldsymbol{x} - \boldsymbol{a}_i\| \\
&\quad f_i = \boldsymbol{c}_i^T(\boldsymbol{x} - \boldsymbol{a}_i), \quad i = 1, \ldots, N \\
&\quad \left\| \begin{bmatrix} \boldsymbol{f} \\ t - 1/4 \end{bmatrix} \right\| \le t + 1/4 \\
&\quad \begin{bmatrix} \boldsymbol{I}_3 & \boldsymbol{x} \\ \boldsymbol{x}^T & z \end{bmatrix} \succeq 0
\end{aligned} \tag{15}$$

The proposed estimator in (15) denoted as "SDP/SOCP1" can be efficiently solved by CVX [27]. Standard semi-definite/second-order cone programming problem (SD/SOCP) solvers like SeDuMi [28] and SDPT3 [29] can be used to solve the convex optimization problem in MATLAB.

III. COOPERATIVE LOCALIZATION

In this section, we discuss the target localization problem in 3-D cooperative scenarios. Consider a WSN which consists of N anchor nodes and M target nodes, where the locations of the anchor nodes are denoted as $\boldsymbol{a}_1, \boldsymbol{a}_2, \ldots, \boldsymbol{a}_N \in \mathbb{R}^3$, while the locations of the target nodes are denoted as $\boldsymbol{x}_1, \boldsymbol{x}_2, \ldots, \boldsymbol{x}_M \in \mathbb{R}^3$.

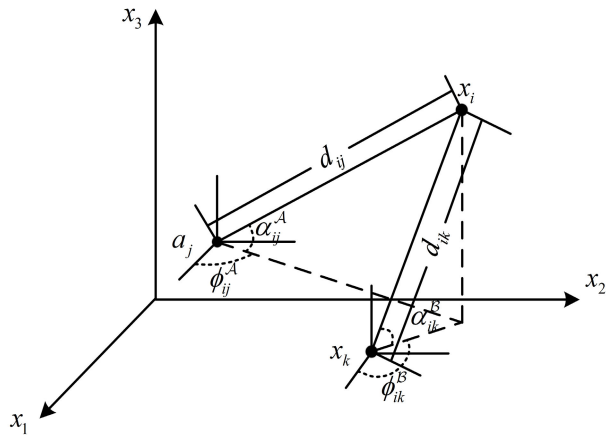

FIGURE 2. The ith target node, the jth anchor node, and the kth target node link in a cooperative scenario.

Fig. 2 shows the ith target node, the jth anchor node, and the kth target node link in a cooperative scenario.

The target/anchor and target/target path loss models are given by [22], [30], [31]

$$L_{ij}^{\mathcal{A}} = L_0 + 10\gamma \log_{10}\left(\frac{\|\boldsymbol{x}_i - \boldsymbol{a}_j\|}{d_0}\right) + n_{ij}, \quad (i,j) \in \mathcal{A} \tag{16a}$$

$$L_{ik}^{\mathcal{B}} = L_0 + 10\gamma \log_{10}\left(\frac{\|\boldsymbol{x}_i - \boldsymbol{x}_k\|}{d_0}\right) + n_{ik}, \quad (i,k) \in \mathcal{B} \tag{16b}$$

where $L_{ij}^{\mathcal{A}}$ and $L_{ik}^{\mathcal{B}}$ are, respectively, the path loss from the ith target node to the jth anchor node, the path loss from the ith target node to the kth target node, L_0 denotes the reference path loss value at the reference distance d_0, γ denotes the PLE, n_{ij} and n_{ik} represent the log-normal shadowing effect, following the identically independent distributed Gaussian distribution, $n_{ij} \sim \mathcal{N}(0, \sigma_{n_{ij}}^2)$, $n_{ik} \sim \mathcal{N}(0, \sigma_{n_{ik}}^2)$. The sets consisting of the target/anchor and target/target connections index pairs within the effective communication range are denoted as $\mathcal{A} = \{(i,j) | \|\boldsymbol{x}_i - \boldsymbol{a}_j\| \le R,\ i = 1, 2, \ldots, M, j = 1, 2, \ldots, N\}$, $\mathcal{B} = \{(i,k) | \|\boldsymbol{x}_i - \boldsymbol{x}_k\| \le R,\ i, k = 1, 2, \ldots, M, i \ne k\}$, respectively. For simplicity and without loss of generality, we assume that the target/target path loss measurements are symmetric, and that all sensors have identical reference path loss value L_0 and communication range R.

As shown in Fig. 2, the azimuth angle and elevation angle measurements are modeled respectively as follows

$$\phi_{ij}^{\mathcal{A}} = \arctan\left(\frac{x_{i2} - a_{j2}}{x_{i1} - a_{j1}}\right) + m_{ij}, \quad (i,j) \in \mathcal{A} \tag{17a}$$

$$\phi_{ik}^{\mathcal{B}} = \arctan\left(\frac{x_{i2} - x_{k2}}{x_{i1} - x_{k1}}\right) + m_{ik}, \quad (i,k) \in \mathcal{B} \tag{17b}$$

$$\alpha_{ij}^{\mathcal{A}} = \arccos\left(\frac{x_{i3} - a_{j3}}{\|\boldsymbol{x}_i - \boldsymbol{a}_j\|}\right) + v_{ij}, \quad (i,j) \in \mathcal{A} \tag{18a}$$

$$\alpha_{ik}^{\mathcal{B}} = \arccos\left(\frac{x_{i3} - x_{k3}}{\|\boldsymbol{x}_i - \boldsymbol{x}_k\|}\right) + v_{ik}, \quad (i,k) \in \mathcal{B} \tag{18b}$$

where m_{ij}, m_{ik} and v_{ij}, v_{ik} represent the measurement errors of the azimuth angle and elevation angle, respectively, modeled as zero-mean Gaussian random variables, *i.e.*, $m_{ij} \sim \mathcal{N}(0, \sigma_{m_{ij}}^2)$, $m_{ik} \sim \mathcal{N}(0, \sigma_{m_{ik}}^2)$ and $v_{ij} \sim \mathcal{N}(0, \sigma_{v_{ij}}^2)$, $v_{ik} \sim \mathcal{N}(0, \sigma_{v_{ik}}^2)$. $\phi_{ij}^{\mathcal{A}}$, $\alpha_{ij}^{\mathcal{A}}$ respectively represent the azimuth angle and elevation angle between the ith target and the jth anchor, $\phi_{ik}^{\mathcal{B}}, \alpha_{ik}^{\mathcal{B}}$ respectively represent the azimuth angle and elevation angle between the ith target and the kth target.

For ease of presentation, here we define $\boldsymbol{x} = [\boldsymbol{x}_1^T, \boldsymbol{x}_2^T, \ldots, \boldsymbol{x}_M^T]^T$.

Moving L_0 to the left side of equation (16), dividing both sides by 10γ, and then taking the power of 10 gives

$$10^{\frac{L_0 - L_{ij}^{\mathcal{A}}}{10\gamma}} \|\boldsymbol{x}_i - \boldsymbol{a}_j\| = d_0 10^{-\frac{n_{ij}}{10\gamma}}, \quad (i,j) \in \mathcal{A} \tag{19a}$$

$$10^{\frac{L_0 - L_{ik}^{\mathcal{B}}}{10\gamma}} \|\boldsymbol{x}_i - \boldsymbol{x}_k\| = d_0 10^{-\frac{n_{ik}}{10\gamma}}, \quad (i,k) \in \mathcal{B} \tag{19b}$$

Similar to the method in Section II, the right side of equation (19) can be approximated by applying the first-order Taylor expansion as follows

$$10^{-\frac{n_{ij}}{10\gamma}} \approx 1 - \frac{\ln(10)}{10\gamma} n_{ij}, \quad (i,j) \in \mathcal{A} \tag{20a}$$

$$10^{-\frac{n_{ik}}{10\gamma}} \approx 1 - \frac{\ln(10)}{10\gamma} n_{ik}, \quad (i,k) \in \mathcal{B} \tag{20b}$$

Substituting (20) into (19), we have

$$b_{ij}^{\mathcal{A}}\|\boldsymbol{x}_i-\boldsymbol{a}_j\| \approx d_0+\xi_{ij}^1, \quad (i,j)\in\mathcal{A} \tag{21a}$$
$$b_{ik}^{\mathcal{B}}\|\boldsymbol{x}_i-\boldsymbol{x}_k\| \approx d_0+\xi_{ik}^1, \quad (i,k)\in\mathcal{B} \tag{21b}$$

where $b_{ij}^{\mathcal{A}}=10^{\frac{L_0-L_{ij}^{\mathcal{A}}}{10\gamma}}$, $b_{ik}^{\mathcal{B}}=10^{\frac{L_0-L_{ik}^{\mathcal{B}}}{10\gamma}}$, $\xi_{ij}^1=-d_0\frac{\ln(10)}{10\gamma}n_{ij}$, $\xi_{ik}^1=-d_0\frac{\ln(10)}{10\gamma}n_{ik}$.

Moving ξ_{ij}^1, ξ_{ik}^1 to the left side of equation (21), squaring both sides and omitting the second-order noise term, we have

$$\xi_{ij}^1 \approx \frac{b_{ij}^{\mathcal{A}^{-1}}(b_{ij}^{\mathcal{A}^2}\|\boldsymbol{x}_i-\boldsymbol{a}_j\|^2-d_0^2)}{2\|\boldsymbol{x}_i-\boldsymbol{a}_j\|}, \quad (i,j)\in\mathcal{A} \tag{22a}$$
$$\xi_{ik}^1 \approx \frac{b_{ik}^{\mathcal{B}^{-1}}(b_{ik}^{\mathcal{B}^2}\|\boldsymbol{x}_i-\boldsymbol{x}_k\|^2-d_0^2)}{2\|\boldsymbol{x}_i-\boldsymbol{x}_k\|}, \quad (i,k)\in\mathcal{B} \tag{22b}$$

Similarly, (17) can be approximately expressed as

$$\xi_{ij}^2 \approx \boldsymbol{c}_{ij}^T(\boldsymbol{x}_i-\boldsymbol{a}_j), (i,j)\in\mathcal{A} \tag{23a}$$
$$\xi_{ik}^2 \approx \boldsymbol{c}_{ik}^T(\boldsymbol{x}_i-\boldsymbol{x}_k), (i,k)\in\mathcal{B} \tag{23b}$$

with $\boldsymbol{c}_{ij}=[-\sin\phi_{ij}^{\mathcal{A}},\cos\phi_{ij}^{\mathcal{A}},0]^T$, $\boldsymbol{c}_{ik}=[-\sin\phi_{ik}^{\mathcal{B}},\cos\phi_{ik}^{\mathcal{B}},0]^T$, ξ_{ij}^2 and ξ_{ik}^2 are weighted noise terms.

As for (18), taking cosine on both sides, and then applying the first-order Taylor expansion, we have

$$\boldsymbol{k}^T(\boldsymbol{x}_i-\boldsymbol{a}_j)\approx\|\boldsymbol{x}_i-\boldsymbol{a}_j\|\cos\alpha_{ij}^{\mathcal{A}}+\xi_{ij}^3, \quad (i,j)\in\mathcal{A} \tag{24a}$$
$$\boldsymbol{k}^T(\boldsymbol{x}_i-\boldsymbol{x}_k)\approx\|\boldsymbol{x}_i-\boldsymbol{x}_k\|\cos\alpha_{ik}^{\mathcal{B}}+\xi_{ik}^3, \quad (i,k)\in\mathcal{B} \tag{24b}$$

where $\boldsymbol{k}=[0,0,1]^T$, ξ_{ij}^3 and ξ_{ik}^3 are weighted noise terms.

According to the squared range criterion (SR) [32], in the following derivation, we apply the least squares methodology to the squared range measurements

$$\cos^2(\alpha_{ij}^{\mathcal{A}})\|\boldsymbol{x}_i-\boldsymbol{a}_j\|^2\approx\boldsymbol{k}^T(\boldsymbol{x}_i-\boldsymbol{a}_j)(\boldsymbol{x}_i-\boldsymbol{a}_j)^T\boldsymbol{k}, \quad (i,j)\in\mathcal{A} \tag{25a}$$
$$\cos^2(\alpha_{ik}^{\mathcal{B}})\|\boldsymbol{x}_i-\boldsymbol{x}_k\|^2\approx\boldsymbol{k}^T(\boldsymbol{x}_i-\boldsymbol{x}_k)(\boldsymbol{x}_i-\boldsymbol{x}_k)^T\boldsymbol{k}, \quad (i,k)\in\mathcal{B} \tag{25b}$$

Based on (22), (23), and (25), we obtain the following LS estimator

$$\begin{aligned}\min_{\boldsymbol{x}} &\sum_{(i,j)\in\mathcal{A}}\left[\frac{b_{ij}^{\mathcal{A}^{-1}}(b_{ij}^{\mathcal{A}^2}\|\boldsymbol{x}_i-\boldsymbol{a}_j\|^2-d_0^2)}{2\|\boldsymbol{x}_i-\boldsymbol{a}_j\|}\right]^2\\ &+\sum_{(i,j)\in\mathcal{A}}\left[\boldsymbol{c}_{ij}^T(\boldsymbol{x}_i-\boldsymbol{a}_j)\right]^2\\ &+\sum_{(i,j)\in\mathcal{A}}\Big[\cos^2(\alpha_{ij}^{\mathcal{A}})\|\boldsymbol{x}_i-\boldsymbol{a}_j\|^2\\ &\qquad-\boldsymbol{k}^T(\boldsymbol{x}_i-\boldsymbol{a}_j)(\boldsymbol{x}_i-\boldsymbol{a}_j)^T\boldsymbol{k}\Big]^2\\ &+\sum_{(i,k)\in\mathcal{B}}\left[\frac{b_{ik}^{\mathcal{B}^{-1}}(b_{ik}^{\mathcal{B}^2}\|\boldsymbol{x}_i-\boldsymbol{x}_k\|^2-d_0^2)}{2\|\boldsymbol{x}_i-\boldsymbol{x}_k\|}\right]^2\\ &+\sum_{(i,k)\in\mathcal{B}}\left[\boldsymbol{c}_{ik}^T(\boldsymbol{x}_i-\boldsymbol{x}_k)\right]^2\\ &+\sum_{(i,k)\in\mathcal{B}}\Big[\cos^2(\alpha_{ik}^{\mathcal{B}})\|\boldsymbol{x}_i-\boldsymbol{x}_k\|^2\\ &\qquad-\boldsymbol{k}^T(\boldsymbol{x}_i-\boldsymbol{x}_k)(\boldsymbol{x}_i-\boldsymbol{x}_k)^T\boldsymbol{k}\Big]^2\end{aligned} \tag{26}$$

Introducing auxiliary variables $\boldsymbol{f},\hat{\boldsymbol{f}},\boldsymbol{g},\hat{\boldsymbol{g}}$, problem (26) can be written equivalently as follows

$$\begin{aligned}\min_{\boldsymbol{x},\boldsymbol{f},\hat{\boldsymbol{f}},\boldsymbol{g},\hat{\boldsymbol{g}}} &\sum_{(i,j)\in\mathcal{A}}\left[\frac{b_{ij}^{\mathcal{A}^{-1}}(b_{ij}^{\mathcal{A}^2}\|\boldsymbol{E}_i^T\boldsymbol{x}-\boldsymbol{a}_j\|^2-d_0^2)}{2\|\boldsymbol{E}_i^T\boldsymbol{x}-\boldsymbol{a}_j\|}\right]^2\\ &+\sum_{(i,j)\in\mathcal{A}}f_{ij}^2+\sum_{(i,j)\in\mathcal{A}}g_{ij}^2\\ &+\sum_{(i,k)\in\mathcal{B}}\left[\frac{b_{ik}^{\mathcal{B}^{-1}}(b_{ik}^{\mathcal{B}^2}\|\boldsymbol{E}_i^T\boldsymbol{x}-\boldsymbol{E}_k^T\boldsymbol{x}\|^2-d_0^2)}{2\|\boldsymbol{E}_i^T\boldsymbol{x}-\boldsymbol{E}_k^T\boldsymbol{x}\|}\right]^2\\ &+\sum_{(i,k)\in\mathcal{B}}\hat{f}_{ik}^2+\sum_{(i,k)\in\mathcal{B}}\hat{g}_{ik}^2\\ \text{s.t. } & g_{ij}=\cos^2(\alpha_{ij}^{\mathcal{A}})\|\boldsymbol{E}_i^T\boldsymbol{x}-\boldsymbol{a}_j\|^2\\ &-\boldsymbol{k}^T(\boldsymbol{E}_i^T\boldsymbol{x}-\boldsymbol{a}_j)(\boldsymbol{E}_i^T\boldsymbol{x}-\boldsymbol{a}_j)^T\boldsymbol{k}\\ & f_{ij}=\boldsymbol{c}_{ij}^T(\boldsymbol{E}_i^T\boldsymbol{x}-\boldsymbol{a}_j), \quad (i,j)\in\mathcal{A}\\ & \hat{g}_{ik}=\cos^2(\alpha_{ik}^{\mathcal{B}})\|\boldsymbol{E}_i^T\boldsymbol{x}-\boldsymbol{E}_k^T\boldsymbol{x}\|^2\\ &-\boldsymbol{k}^T(\boldsymbol{E}_i^T\boldsymbol{x}-\boldsymbol{E}_k^T\boldsymbol{x})(\boldsymbol{E}_i^T\boldsymbol{x}-\boldsymbol{E}_k^T\boldsymbol{x})^T\boldsymbol{k}\\ & \hat{f}_{ik}=\boldsymbol{c}_{ik}^T(\boldsymbol{E}_i^T\boldsymbol{x}-\boldsymbol{E}_k^T\boldsymbol{x}), \quad (i,k)\in\mathcal{B}\end{aligned} \tag{27}$$

where $\boldsymbol{E}_i=\boldsymbol{e}_i\bigotimes\boldsymbol{I}_3$, $\boldsymbol{e}_i$ denotes the ith column of the M-dimensional identity matrix, and $\bigotimes$ denotes Kronecker product.

By stacking the variables $\boldsymbol{f}$, $\hat{\boldsymbol{f}}$, $\boldsymbol{g}$, $\hat{\boldsymbol{g}}$ into a vector $\boldsymbol{z}$, and introducing the slack variables $\boldsymbol{e}$, $\hat{\boldsymbol{e}}$, t, we have

$$\begin{aligned}\min_{\boldsymbol{x},\boldsymbol{e},\hat{\boldsymbol{e}},\boldsymbol{z},t} &\sum_{(i,j)\in\mathcal{A}}e_{ij}+\sum_{(i,k)\in\mathcal{B}}\hat{e}_{ik}+t\\ \text{s.t. } &\left[\frac{b_{ij}^{\mathcal{A}^{-1}}(b_{ij}^{\mathcal{A}^2}\|\boldsymbol{E}_i^T\boldsymbol{x}-\boldsymbol{a}_j\|^2-d_0^2)}{2\|\boldsymbol{E}_i^T\boldsymbol{x}-\boldsymbol{a}_j\|}\right]^2\le e_{ij}, \quad (i,j)\in\mathcal{A}\\ &\left[\frac{b_{ik}^{\mathcal{B}^{-1}}(b_{ik}^{\mathcal{B}^2}\|\boldsymbol{E}_i^T\boldsymbol{x}-\boldsymbol{E}_k^T\boldsymbol{x}\|^2-d_0^2)}{2\|\boldsymbol{E}_i^T\boldsymbol{x}-\boldsymbol{E}_k^T\boldsymbol{x}\|}\right]^2\le\hat{e}_{ik}, \quad (i,k)\in\mathcal{B}\\ &\|\boldsymbol{z}\|^2\le t\end{aligned} \tag{28}$$

Inequality constraints in (28) can be converted to second-order cones, and according to $trace(\boldsymbol{x}\boldsymbol{x}^T)=\boldsymbol{x}^T\boldsymbol{x}$, we have

$$\begin{aligned}\min_{\substack{\boldsymbol{X},\boldsymbol{x},\boldsymbol{z},t\\ \boldsymbol{e},\hat{\boldsymbol{e}},\boldsymbol{R},\hat{\boldsymbol{R}}}} &\sum_{(i,j)\in\mathcal{A}}e_{ij}+\sum_{(i,k)\in\mathcal{B}}\hat{e}_{ik}+t\\ \text{s.t. } & R_{ij}=trace(\boldsymbol{E}_i^T\boldsymbol{X}\boldsymbol{E}_i)-2\boldsymbol{a}_j^T\boldsymbol{E}_i^T\boldsymbol{x}+\|\boldsymbol{a}_j\|^2\\ &\left\|\begin{bmatrix}b_{ij}^{\mathcal{A}^{-1}}(b_{ij}^{\mathcal{A}^2}R_{ij}-d_0^2)\\ R_{ij}-e_{ij}\end{bmatrix}\right\|\le R_{ij}+e_{ij}, \quad (i,j)\in\mathcal{A}\\ &\hat{R}_{ik}=trace(\boldsymbol{E}_i^T\boldsymbol{X}\boldsymbol{E}_i)-2trace(\boldsymbol{E}_i^T\boldsymbol{X}\boldsymbol{E}_k)\\ &+trace(\boldsymbol{E}_k^T\boldsymbol{X}\boldsymbol{E}_k)\end{aligned}$$

$$\left\| \begin{bmatrix} b_{ik}^{\mathcal{B}^{-1}}(b_{ik}^{\mathcal{B}^2}\hat{R}_{ik} - d_0^2) \\ \hat{R}_{ik} - \hat{e}_{ik} \end{bmatrix} \right\| \leq \hat{R}_{ik} + \hat{e}_{ik}, \quad (i,k) \in \mathcal{B}$$
$$\left\| \begin{bmatrix} z \\ t - 1/4 \end{bmatrix} \right\| \leq t + 1/4$$
$$\boldsymbol{X} = \boldsymbol{x}\boldsymbol{x}^T \tag{29}$$

By relaxing $\boldsymbol{X} = \boldsymbol{x}\boldsymbol{x}^T$ to $\boldsymbol{X} \succeq \boldsymbol{x}\boldsymbol{x}^T$, and applying Schur complement [26] to transform the constraint into the form of linear matrix inequality (LMI), we obtain a convex problem (30)

$$\begin{aligned}
&\min_{\boldsymbol{X},\boldsymbol{x},z,t,\boldsymbol{e},\hat{\boldsymbol{e}},\boldsymbol{R},\hat{\boldsymbol{R}}} \sum_{(i,j)\in\mathcal{A}} e_{ij} + \sum_{(i,k)\in\mathcal{B}} \hat{e}_{ik} + t \\
&\text{s.t. } R_{ij} = trace(\boldsymbol{E}_i^T\boldsymbol{X}\boldsymbol{E}_i) - 2\boldsymbol{a}_j^T\boldsymbol{E}_i^T\boldsymbol{x} + \|\boldsymbol{a}_j\|^2 \\
&\left\| \begin{bmatrix} b_{ij}^{\mathcal{A}^{-1}}(b_{ij}^{\mathcal{A}^2}R_{ij} - d_0^2) \\ R_{ij} - e_{ij} \end{bmatrix} \right\| \leq R_{ij} + e_{ij}, \quad (i,j) \in \mathcal{A} \\
&\hat{R}_{ik} = trace(\boldsymbol{E}_i^T\boldsymbol{X}\boldsymbol{E}_i) - 2trace(\boldsymbol{E}_i^T\boldsymbol{X}\boldsymbol{E}_k) \\
&\quad + trace(\boldsymbol{E}_k^T\boldsymbol{X}\boldsymbol{E}_k) \\
&\left\| \begin{bmatrix} b_{ik}^{\mathcal{B}^{-1}}(b_{ik}^{\mathcal{B}^2}\hat{R}_{ik} - d_0^2) \\ \hat{R}_{ik} - \hat{e}_{ik} \end{bmatrix} \right\| \leq \hat{R}_{ik} + \hat{e}_{ik}, \quad (i,k) \in \mathcal{B} \\
&\left\| \begin{bmatrix} z \\ t - 1/4 \end{bmatrix} \right\| \leq t + 1/4 \\
&\begin{bmatrix} \boldsymbol{X} & \boldsymbol{x} \\ \boldsymbol{x}^T & 1 \end{bmatrix} \succeq 0
\end{aligned} \tag{30}$$

The proposed estimator in (30) is a mixed semi-definite/second-order cone programming problem, which is referred to as "SDP/SOCP2" in the following sections.

IV. COMPLEXITY ANALYSIS

The trade-off between accuracy and complexity is one of the criteria on the applicability of the algorithm. We assume that there is a communication link between any node in the network to analyze the worst-case complexity, *i.e.*, the total number of links in the network is $L = |\mathcal{A}| + |\mathcal{B}|$, where $|\mathcal{A}| = MN, |\mathcal{B}| = M(M-1)/2$. Complexity can be expressed as a function of L, M, N. In noncooperative scenarios, $M = 1$. The results in [33] are applied to analyze the worst-case complexities of the methods considered in this paper

$$\mathcal{O}\left(\sqrt{\mu}\left(m\sum_{i=1}^{N_{sd}} n_i^{sd^3} + m^2\sum_{i=1}^{N_{sd}} n_i^{sd^2} + m^2\sum_{i=1}^{N_{soc}} n_i^{soc} + \sum_{i=1}^{N_{soc}} n_i^{soc^2} + m^3\right)\right) \tag{31}$$

where m is the number of equality constraints, N_{soc}, N_{sd} are respectively the number of second-order cone constraints and semi-definite cone constraints, n_i^{soc}, n_i^{sd} are respectively the dimensions of the ith second-order cone and the ith semi-definite cone, $\mu = \sum_{i=1}^{N_{sd}} n_i^{sd} + 2N_{soc}$ is the so-called barrier parameter.

Table 1, Table 2 respectively show the complexities of the algorithms considered in this paper for noncooperative and cooperative localization scenarios. Assuming that $K = 30$ is the maximum number of steps in the bisection procedure applied in [34].

TABLE 1. Summary of the considered methods for noncooperative scenarios.

Method	Description	Complexity
GTRS	The generalized trust region subproblem method in [34]	$\mathcal{O}(K_{max}N)$
WLS	The weighted least squares method in [35]	$\mathcal{O}(N)$
SDP/SOCP1	The proposed method in II	$\mathcal{O}(N^{3.5})$

TABLE 2. Summary of the considered methods for cooperative scenarios.

Method	Description	Complexity
SDP-RSS	The method in [20]	$\mathcal{O}\left(M^{0.5}\left(4M^4\left(N+\frac{M}{2}\right)^2\right)\right)$
SDP	The method in [22]	$\mathcal{O}\left((3M)^{0.5}\left(81M^4\left(N+\frac{M}{2}\right)^2\right)\right)$
SDP/SOCP2	The proposed method in III	$\mathcal{O}\left((3M)^{0.5}\left(81M^4\left(N+2M\right)^2\right)\right)$

The above two tables show that the complexities of the algorithms mainly depend on the scale of the wireless sensor network. Observing Table 1, since the bisection procedure is adopted, the GTRS method is slightly more complex than the WLS method, but the subsequent simulation results show that the estimation accuracy of GTRS is better than that of WLS under various settings. Although the SDP/SOCP1 method has the highest complexity among the considered methods, it has the best performance. Table 2 shows the algorithms using hybrid measurements are slightly more complex than the algorithms using a single kind of measurement, but can greatly reduce the estimation error.

V. CRAMER-RAO LOWER BOUND ANALYSIS

The CRLB is generally used as a benchmark to verify the performance of the localization algorithms. Although the CRLB for a single kind of measurement is widely discussed, there is no report about the CRLB on hybrid measurements in the cooperative case, which will be discussed in this section.

In the cooperative scenarios, the CRLB for the ith component of the estimated parameter $\boldsymbol{x}$ is given by

$$CRLB(\hat{x}_i) = [\mathcal{F}^{-1}]_{i,i} \tag{32}$$

where $\mathcal{F}$ is the Fisher information matrix (FIM) [36], the elements in the FIM are defined as follows

$$[\mathcal{F}]_{i,j} = -\mathbb{E}\left[\frac{\partial^2 lnp(\boldsymbol{L}|\boldsymbol{x})}{\partial[\boldsymbol{x}]_i \partial[\boldsymbol{x}]_j}\right] \tag{33}$$

where $\boldsymbol{L}$ is the observation vector, and $p(\boldsymbol{L}|\boldsymbol{x})$ is the conditional probability density function (pdf).

Accordingly, the CRLB for the estimate of the target positions $\boldsymbol{x}$ is formulated as

$$CRLB = trace([\mathcal{F}^{-1}(\boldsymbol{x})]) \tag{34}$$

We omit the closed-form formulas of the elements in $\mathcal{F}$ here due to their complex expressions. The detailed derivation and expression of each element in the FIM are given in Appendix.

VI. SIMULATION RESULTS

In this section, we perform a series of simulations by setting different scenarios to verify the performance of the proposed algorithms. The CRLB on the RMSE of any unbiased estimator is employed as a performance benchmark, and the RMSE is used as the main performance indicator of localization algorithms. To verify the benefits of fusing two measurements, in the cooperative scenarios, the SDP/SOCP2 method based on hybrid RSS-AOA measurements is compared with the SDP-RSS method based on RSS measurements.

A. NONCOOPERATIVE LOCALIZATION

In the noncooperative WSNs, the models (1), (2), (3) are used to generate the RSS and AOA measurements. We assume that both the target and the anchor nodes are randomly deployed in a region of size $15\times15\times15m^3$ in each Monte Carlo (Mc) run, the reference distance $d_0 = 1m$, the path loss $L_0 = 40$dB, and the PLE is fixed as $\gamma = 2.5$, similar to [20], the true PLE for each link follows a uniform distribution with an interval $\gamma \sim \mathcal{U}[2.2,2.8]$. The proposed method is implemented by MATLAB package CVX using SeDuMi as the solver, for the noncooperative scenarios, RMSE $= \sqrt{\sum_{i=1}^{Mc} \frac{\|\boldsymbol{x}_i-\hat{\boldsymbol{x}}_i\|^2}{Mc}}$, where $\hat{\boldsymbol{x}}_i$ is the estimated location of the target in the ith Monte Carlo run, $M_c = 4000$.

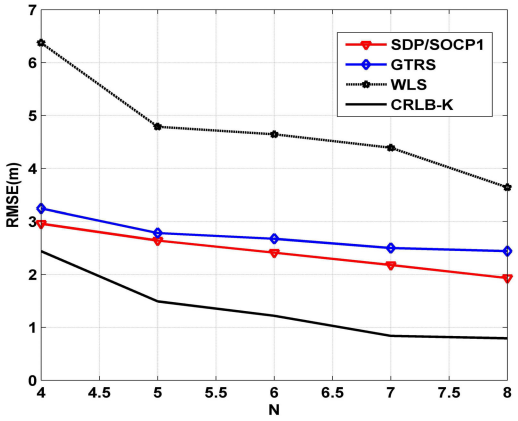

FIGURE 3. RMSE versus the number of anchor nodes N comparison.

Fig. 3 shows the RMSE versus the number of anchor nodes N when $\sigma_n = 6$dB, $\sigma_m = 5$deg, $\sigma_v = 5$deg. The figure shows that the estimation accuracy of the discussed algorithms is improved as the number of anchor nodes increases due to more available information in the network. Additionally, the SDP/SOCP1 method outperforms the other discussed methods and is closer to the CRLB for each N. We also observe that the margin between SDP/SOCP1 and GTRS increases as N grows, which verifies the superior performance of the proposed method.

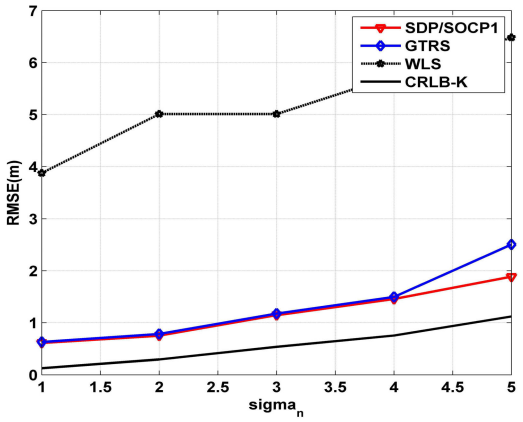

FIGURE 4. RMSE versus σ_n(dB) comparison.

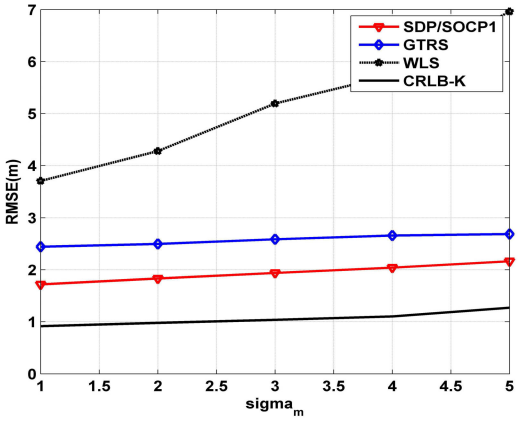

FIGURE 5. RMSE versus σ_m(deg) comparison.

Fig. 4 shows the RMSE versus σ_n(dB) when $\sigma_m = \sigma_v = 5$deg, $N = 6$. The figure shows that the estimation accuracy of the SDP/SOCP1 method is slightly better than that of the GTRS method as σ_n varies from 1 to 4dB, and when $\sigma_n = 5$dB, our estimator has outstanding performance. The effects of two other measurement noises on the RMSE of the estimators under consideration are also studied. Fig. 5 shows the RMSE versus σ_m(deg) when $\sigma_n = 6$dB, $\sigma_v = 5$deg, $N = 6$. Observing that the SDP/SOCP1 method and the GTRS method are more robust when the measurements deteriorate. Fig. 6 shows the RMSE versus σ_v(deg) when $\sigma_n = 6$dB, $\sigma_m = 5$deg, $N = 6$. Finding that the margin between SDP/SOCP1 and GTRS is slowly increasing when σ_v varies from 2 to 5deg. From the above three figures we know that the performance of the discussed algorithms deteriorates as the quality of the measurements decreases. Furthermore, the SDP/SOCP1 method is less affected by the quality of the AOA measurements and is more affected by the quality of the RSS measurements. Additionally, the proposed method provides superior performance over the other discussed methods and is closer to the CRLB in all noise cases.

B. COOPERATIVE LOCALIZATION

In the cooperative WSNs, the models (16), (17), (18) are used to generate the RSS and AOA measurements. We assume that

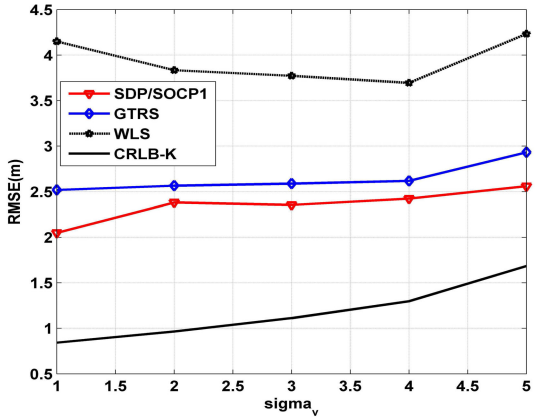

FIGURE 6. RMSE versus σ_v (deg) comparison.

both the anchor and the target nodes are randomly deployed in a region of size $30 \times 30 \times 30\ m^3$ in each Monte Carlo (Mc) run, the reference distance $d_0 = 1m$, the reference path loss $L_0 = 40$dB, the communication distance $R = 8m$, and the PLE is fixed as $\gamma = 2.5$, the true PLE for each link follows a uniform distribution with an interval $\gamma \sim \mathcal{U}[2.2,2.8]$, for the cooperative scenarios, the RMSE is calculated by averaging over all the estimated locations of the target nodes and noise realizations, *i.e.*, RMSE $= \sqrt{\sum_{i=1}^{Mc}\sum_{j=1}^{M}\frac{\|\boldsymbol{x}_{ij}-\hat{\boldsymbol{x}}_{ij}\|^2}{MMc}}$, where $\hat{\boldsymbol{x}}_{ij}$ is the estimated location of the jth target in the ith Monte Carlo (Mc) run, $M_c = 2000$.

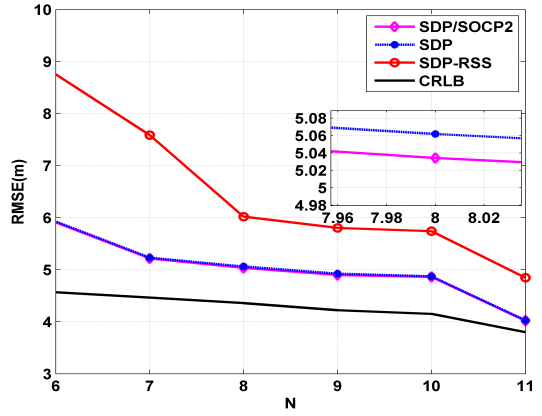

FIGURE 7. RMSE versus the number of anchor nodes N comparison.

Fig. 7 shows the RMSE versus the number of anchor nodes N when $\sigma_n = 5$dB, $\sigma_m = \sigma_v = 4$deg, $M = 25$. It is observed that the performance of the discussed methods is improved as N increases, and since the AOA measurements and RSS measurements can provide more information, the hybrid algorithms have excellent performance and are close to the CRLB. Furthermore, adequate information in the network decreases the performance margin between the SDP/SOCP2 method and the SDP method, one can see that the new method outperforms the existing method by roughly $0.02m$ when $N = 8$, however, when compared with the SDP-RSS method, the new method has significant performance, reducing the estimation error by roughly $3.6m$ when $N = 7$, which confirms that the algorithms using hybrid measurements have better performance than the algorithms using a single kind of measurement.

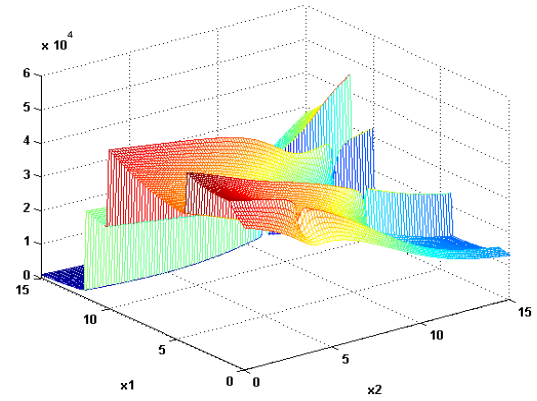

FIGURE 8. The objective function of the ML estimator versus x_1 and x_2 coordinates.

In the following simulations, we compare the surface shapes of objective function between maximum likelihood (ML) [35] and proposed SDP/SOCP1 estimator.

A target node and four anchor nodes are randomly deployed in a region of size $15 \times 15 \times 15\ m^3$, $\sigma_n = 3$dB, $\sigma_m = \sigma_v = 3$deg, $\gamma = 2.5$, $L_0 = 40$dB, and $d_0 = 1m$. In this example, we have three unknown parameters, it is not possible to show a plot in four-dimensional space. So Fig. 8 and Fig. 9 respectively show the surface shapes of the ML estimator and the function in (10) versus x_1 and x_2 coordinates when x_3 is fixed at the true value.

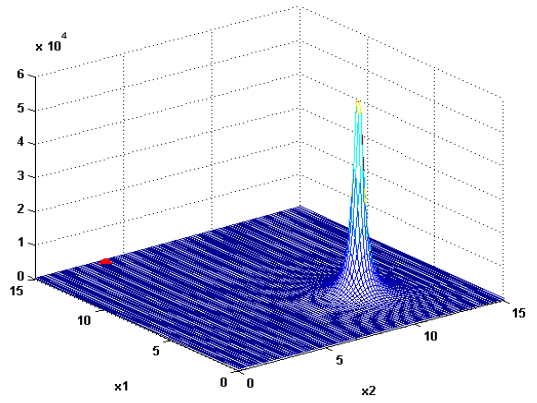

FIGURE 9. The objective function in (10) versus x_1 and x_2 coordinates.

Fig. 8 shows that the objective function of the ML estimator has many local minima and saddle points, it's not easy to find the optimal solution, while the objective function in (10), shown in Fig.9, is much smoother than that of the ML estimator and has a global minimum at $[14.55, 3.64, 10.14]m$ which is indicated by a red point (the target is located at $[14.37, 3.61, 10.14]m$). Simulations for the other two cases have similar results.

From these figures, we conclude that the objective function of the ML estimator based on hybrid measurements has many local optima, its globally optimal solution is very hard to obtain. However, the advantage of our method is that the convergence to the globally optimal solution is guaranteed.

VII. CONCLUSION

In this paper, we propose the target localization methods based on hybrid RSS-AOA measurements in both noncooperative and cooperative 3-D WSNs. According to LS criterion, the target localization problems are expressed as the minimization problems, then we relax the original non-convex problems into convex problems by using semi-definite relaxation and second-order cone relaxation techniques, the convex problems can be effectively solved by the interior point method. It can be observed from our simulation results that the hybrid estimators can achieve higher estimation accuracy than the estimators based on a single kind of measurement, and the results also depict that the proposed methods exhibit exceeding performance in all considered scenarios and robustness to inaccuracy PLE. However, we only address the localization problems for the case of known transmit power, our next work is to extend the methods to the unknown transmit power case and derive the corresponding CRLB.

APPENDIX

Based on the information from Section V, the CRLB for the estimated target positions is given in this section. To facilitate the derivation of the CRLB, here we redefine $\boldsymbol{x} = [\boldsymbol{x}_1, \boldsymbol{x}_2, \ldots, \boldsymbol{x}_M]$ as a $3 \times M$ matrix, and it is obvious that $\mathcal{F} \in \mathbb{S}^{3M}$. Due to the nature of symmetric matrix, we only derive some elements of the FIM as follows

$$
\begin{aligned}
[\mathcal{F}]_{i,i} = & \sum_{\{j|(i,j)\in\mathcal{A}\}} \left(\frac{10\gamma}{ln(10)}\right)^2 \frac{1}{\sigma_{n_{ij}}^2} \frac{(x_{i1}-a_{j1})^2}{\|\boldsymbol{x}_i-\boldsymbol{a}_j\|^4} \\
& + \sum_{\{j|(i,j)\in\mathcal{A}\}} \frac{1}{\sigma_{m_{ij}}^2} \frac{(x_{i2}-a_{j2})^2}{\|\boldsymbol{x}_{1:2,i}-\boldsymbol{a}_{1:2,j}\|^4} \\
& + \sum_{\{j|(i,j)\in\mathcal{A}\}} \frac{1}{\sigma_{v_{ij}}^2} \frac{(x_{i1}-a_{j1})^2(x_{i3}-a_{j3})^2}{\|\boldsymbol{x}_{1:2,i}-\boldsymbol{a}_{1:2,j}\|^2\|\boldsymbol{x}_i-\boldsymbol{a}_j\|^4} \\
& + \sum_{\{k|(i,k)\in\mathcal{B}\}} \left(\frac{10\gamma}{ln(10)}\right)^2 \frac{1}{\sigma_{n_{ik}}^2} \frac{(x_{i1}-x_{k1})^2}{\|\boldsymbol{x}_i-\boldsymbol{x}_k\|^4} \\
& + \sum_{\{k|(i,k)\in\mathcal{B}\}} \frac{1}{\sigma_{m_{ik}}^2} \frac{(x_{i2}-x_{k2})^2}{\|\boldsymbol{x}_{1:2,i}-\boldsymbol{x}_{1:2,k}\|^4} \\
& + \sum_{\{k|(i,k)\in\mathcal{B}\}} \frac{1}{\sigma_{v_{ik}}^2} \frac{(x_{i1}-x_{k1})^2(x_{i3}-x_{k3})^2}{\|\boldsymbol{x}_{1:2,i}-\boldsymbol{x}_{1:2,k}\|^2\|\boldsymbol{x}_i-\boldsymbol{x}_k\|^4}
\end{aligned}
$$

$$
\begin{aligned}
[\mathcal{F}]_{i,j} = & -\left(\frac{10\gamma}{ln(10)}\right)^2 \frac{1}{\sigma_{n_{ij}}^2} \frac{(x_{i1}-x_{j1})^2}{\|\boldsymbol{x}_i-\boldsymbol{x}_j\|^4} \\
& - \frac{1}{\sigma_{m_{ij}}^2} \frac{(x_{i2}-x_{j2})^2}{\|\boldsymbol{x}_{1:2,i}-\boldsymbol{x}_{1:2,j}\|^4} \\
& - \frac{1}{\sigma_{v_{ij}}^2} \times \frac{(x_{i1}-x_{j1})^2(x_{i3}-x_{j3})^2}{\|\boldsymbol{x}_{1:2,i}-\boldsymbol{x}_{1:2,j}\|^2\|\boldsymbol{x}_i-\boldsymbol{x}_j\|^4}
\end{aligned}
$$

$$
\begin{aligned}
[\mathcal{F}]_{i,M+i} = & \sum_{\{j|(i,j)\in\mathcal{A}\}} \left(\frac{10\gamma}{ln(10)}\right)^2 \frac{1}{\sigma_{n_{ij}}^2} \frac{(x_{i1}-a_{j1})(x_{i2}-a_{j2})}{\|\boldsymbol{x}_i-\boldsymbol{a}_j\|^4} \\
& - \sum_{\{j|(i,j)\in\mathcal{A}\}} \frac{1}{\sigma_{m_{ij}}^2} \frac{(x_{i1}-a_{j1})(x_{i2}-a_{j2})}{\|\boldsymbol{x}_{1:2,i}-\boldsymbol{a}_{1:2,j}\|^4} \\
& + \sum_{\{j|(i,j)\in\mathcal{A}\}} \frac{1}{\sigma_{v_{ij}}^2} \times \frac{(x_{i1}-a_{j1})(x_{i2}-a_{j2})(x_{i3}-a_{j3})^2}{\|\boldsymbol{x}_{1:2,i}-\boldsymbol{a}_{1:2,j}\|^2\|\boldsymbol{x}_i-\boldsymbol{a}_j\|^4} \\
& + \sum_{\{k|(i,k)\in\mathcal{B}\}} \left(\frac{10\gamma}{ln(10)}\right)^2 \frac{1}{\sigma_{n_{ik}}^2} \times \frac{(x_{i1}-x_{k1})(x_{i2}-x_{k2})}{\|\boldsymbol{x}_i-\boldsymbol{x}_k\|^4} \\
& - \sum_{\{k|(i,k)\in\mathcal{B}\}} \frac{1}{\sigma_{m_{ik}}^2} \times \frac{(x_{i1}-x_{k1})(x_{i2}-x_{k2})}{\|\boldsymbol{x}_{1:2,i}-\boldsymbol{x}_{1:2,k}\|^4} \\
& + \sum_{\{k|(i,k)\in\mathcal{B}\}} \frac{1}{\sigma_{v_{ik}}^2} \times \frac{(x_{i1}-x_{k1})(x_{i2}-x_{k2})(x_{i3}-x_{k3})^2}{\|\boldsymbol{x}_{1:2,i}-\boldsymbol{x}_{1:2,k}\|^2\|\boldsymbol{x}_i-\boldsymbol{x}_k\|^4}
\end{aligned}
$$

$$
\begin{aligned}
[\mathcal{F}]_{i,M+j} = & -\left(\frac{10\gamma}{ln(10)}\right)^2 \frac{1}{\sigma_{n_{ij}}^2} \frac{(x_{i1}-x_{j1})(x_{i2}-x_{j2})}{\|\boldsymbol{x}_i-\boldsymbol{x}_j\|^4} \\
& + \frac{1}{\sigma_{m_{ij}}^2} \frac{(x_{i1}-x_{j1})(x_{i2}-x_{j2})}{\|\boldsymbol{x}_{1:2,i}-\boldsymbol{x}_{1:2,j}\|^4} \\
& - \frac{1}{\sigma_{v_{ij}}^2} \frac{(x_{i1}-x_{j1})(x_{i2}-x_{j2})(x_{i3}-x_{j3})^2}{\|\boldsymbol{x}_{1:2,i}-\boldsymbol{x}_{1:2,j}\|^2\|\boldsymbol{x}_i-\boldsymbol{x}_j\|^4}
\end{aligned}
$$

$$
\begin{aligned}
[\mathcal{F}]_{i,2M+i} = & \sum_{\{j|(i,j)\in\mathcal{A}\}} \left(\frac{10\gamma}{ln(10)}\right)^2 \frac{1}{\sigma_{n_{ij}}^2} \frac{(x_{i1}-a_{j1})(x_{i3}-a_{j3})}{\|\boldsymbol{x}_i-\boldsymbol{a}_j\|^4} \\
& - \sum_{\{j|(i,j)\in\mathcal{A}\}} \frac{1}{\sigma_{v_{ij}}^2} \frac{(x_{i1}-a_{j1})(x_{i3}-a_{j3})}{\|\boldsymbol{x}_i-\boldsymbol{a}_j\|^4} \\
& + \sum_{\{k|(i,k)\in\mathcal{B}\}} \left(\frac{10\gamma}{ln(10)}\right)^2 \frac{1}{\sigma_{n_{ik}}^2} \times \frac{(x_{i1}-x_{k1})(x_{i3}-x_{k3})}{\|\boldsymbol{x}_i-\boldsymbol{x}_k\|^4} \\
& - \sum_{\{k|(i,k)\in\mathcal{B}\}} \frac{1}{\sigma_{v_{ik}}^2} \frac{(x_{i1}-x_{k1})(x_{i3}-x_{k3})}{\|\boldsymbol{x}_i-\boldsymbol{x}_k\|^4}
\end{aligned}
$$

$$[\mathcal{F}]_{i,2M+j}$$
$$= -\left(\frac{10\gamma}{ln(10)}\right)^2 \frac{1}{\sigma_{n_{ij}}^2} \frac{(x_{i1}-x_{j1})(x_{i3}-x_{j3})}{\|\boldsymbol{x}_i-\boldsymbol{x}_j\|^4} + \frac{1}{\sigma_{v_{ij}}^2} \frac{(x_{i1}-x_{j1})(x_{i3}-x_{j3})}{\|\boldsymbol{x}_i-\boldsymbol{x}_j\|^4}$$

$$[\mathcal{F}]_{M+i,M+i}$$
$$= \sum_{\{j|(i,j)\in\mathcal{A}\}} \left(\frac{10\gamma}{ln(10)}\right)^2 \frac{1}{\sigma_{n_{ij}}^2} \frac{(x_{i2}-a_{j2})^2}{\|\boldsymbol{x}_i-\boldsymbol{a}_j\|^4} + \sum_{\{j|(i,j)\in\mathcal{A}\}} \frac{1}{\sigma_{m_{ij}}^2} \frac{(x_{i1}-a_{j1})^2}{\|\boldsymbol{x}_{1:2,i}-\boldsymbol{a}_{1:2,j}\|^4} + \sum_{\{j|(i,j)\in\mathcal{A}\}} \frac{1}{\sigma_{v_{ij}}^2} \frac{(x_{i2}-a_{j2})^2(x_{i3}-a_{j3})^2}{\|\boldsymbol{x}_{1:2,i}-\boldsymbol{a}_{1:2,j}\|^2\|\boldsymbol{x}_i-\boldsymbol{a}_j\|^4} + \sum_{\{k|(i,k)\in\mathcal{B}\}} \left(\frac{10\gamma}{ln(10)}\right)^2 \frac{1}{\sigma_{n_{ik}}^2} \frac{(x_{i2}-x_{k2})^2}{\|\boldsymbol{x}_i-\boldsymbol{x}_k\|^4} + \sum_{\{k|(i,k)\in\mathcal{B}\}} \frac{1}{\sigma_{m_{ik}}^2} \frac{(x_{i1}-x_{k1})^2}{\|\boldsymbol{x}_{1:2,i}-\boldsymbol{x}_{1:2,k}\|^4} + \sum_{\{k|(i,k)\in\mathcal{B}\}} \frac{1}{\sigma_{v_{ik}}^2} \frac{(x_{i2}-x_{k2})^2(x_{i3}-x_{k3})^2}{\|\boldsymbol{x}_{1:2,i}-\boldsymbol{x}_{1:2,k}\|^2\|\boldsymbol{x}_i-\boldsymbol{x}_k\|^4}$$

$$[\mathcal{F}]_{M+i,M+j}$$
$$= -\left(\frac{10\gamma}{ln(10)}\right)^2 \frac{1}{\sigma_{n_{ij}}^2} \frac{(x_{i2}-x_{j2})^2}{\|\boldsymbol{x}_i-\boldsymbol{x}_j\|^4} - \frac{1}{\sigma_{m_{ij}}^2} \frac{(x_{i1}-x_{j1})^2}{\|\boldsymbol{x}_{1:2,i}-\boldsymbol{x}_{1:2,j}\|^4} - \frac{1}{\sigma_{v_{ij}}^2} \frac{(x_{i2}-x_{j2})^2(x_{i3}-x_{j3})^2}{\|\boldsymbol{x}_{1:2,i}-\boldsymbol{x}_{1:2,j}\|^2\|\boldsymbol{x}_i-\boldsymbol{x}_j\|^4}$$

$$[\mathcal{F}]_{M+i,2M+i}$$
$$= -\sum_{\{j|(i,j)\in\mathcal{A}\}} \frac{1}{\sigma_{v_{ij}}^2} \frac{(x_{i2}-a_{j2})(x_{i3}-a_{j3})}{\|\boldsymbol{x}_i-\boldsymbol{a}_j\|^4} + \sum_{\{j|(i,j)\in\mathcal{A}\}} \left(\frac{10\gamma}{ln(10)}\right)^2 \frac{1}{\sigma_{n_{ij}}^2} \times \frac{(x_{i2}-a_{j2})(x_{i3}-a_{j3})}{\|\boldsymbol{x}_i-\boldsymbol{a}_j\|^4} + \sum_{\{k|(i,k)\in\mathcal{B}\}} \left(\frac{10\gamma}{ln(10)}\right)^2 \frac{1}{\sigma_{n_{ik}}^2} \times \frac{(x_{i2}-x_{k2})(x_{i3}-x_{k3})}{\|\boldsymbol{x}_i-\boldsymbol{x}_k\|^4} - \sum_{\{k|(i,k)\in\mathcal{B}\}} \frac{1}{\sigma_{v_{ik}}^2} \frac{(x_{i2}-x_{k2})(x_{i3}-x_{k3})}{\|\boldsymbol{x}_i-\boldsymbol{x}_k\|^4}$$

$$[\mathcal{F}]_{M+i,2M+j}$$
$$= -\left(\frac{10\gamma}{ln(10)}\right)^2 \frac{1}{\sigma_{n_{ij}}^2} \frac{(x_{i2}-x_{j2})(x_{i3}-x_{j3})}{\|\boldsymbol{x}_i-\boldsymbol{x}_j\|^4} + \frac{1}{\sigma_{v_{ij}}^2} \frac{(x_{i2}-x_{j2})(x_{i3}-x_{j3})}{\|\boldsymbol{x}_i-\boldsymbol{x}_j\|^4}$$

$$[\mathcal{F}]_{2M+i,2M+i}$$
$$= \sum_{\{j|(i,j)\in\mathcal{A}\}} \left(\frac{10\gamma}{ln(10)}\right)^2 \frac{1}{\sigma_{n_{ij}}^2} \frac{(x_{i3}-a_{j3})^2}{\|\boldsymbol{x}_i-\boldsymbol{a}_j\|^4} + \sum_{\{j|(i,j)\in\mathcal{A}\}} \frac{1}{\sigma_{v_{ij}}^2} \frac{\|\boldsymbol{x}_{1:2,i}-\boldsymbol{a}_{1:2,j}\|^2}{\|\boldsymbol{x}_i-\boldsymbol{a}_j\|^4} + \sum_{\{k|(i,k)\in\mathcal{B}\}} \left(\frac{10\gamma}{ln(10)}\right)^2 \frac{1}{\sigma_{n_{ik}}^2} \frac{(x_{i3}-x_{k3})^2}{\|\boldsymbol{x}_i-\boldsymbol{x}_k\|^4} + \sum_{\{k|(i,k)\in\mathcal{B}\}} \frac{1}{\sigma_{v_{ik}}^2} \frac{\|\boldsymbol{x}_{1:2,i}-\boldsymbol{x}_{1:2,k}\|^2}{\|\boldsymbol{x}_i-\boldsymbol{x}_k\|^4}$$

$$[\mathcal{F}]_{2M+i,2M+j}$$
$$= -\left(\frac{10\gamma}{ln(10)}\right)^2 \frac{1}{\sigma_{n_{ij}}^2} \frac{(x_{i3}-x_{j3})^2}{\|\boldsymbol{x}_i-\boldsymbol{x}_j\|^4} - \frac{1}{\sigma_{v_{ij}}^2} \frac{\|\boldsymbol{x}_{1:2,i}-\boldsymbol{x}_{1:2,j}\|^2}{\|\boldsymbol{x}_i-\boldsymbol{x}_j\|^4},$$
$$i=j=1,\ldots,M, \quad i<j$$

REFERENCES

[1] I. F. Akyildiz, W. Su, Y. Sankarasubramaniam, and E. Cayirci, "Wireless sensor networks: A survey," *Comput. Netw.*, vol. 38, no. 4, pp. 393–422, Mar. 2002.

[2] N. Patwari, J. N. Ash, S. Kyperountas, A. O. Hero, R. L. Moses, and N. S. Correal, "Locating the nodes: Cooperative localization in wireless sensor networks," *IEEE Signal Process. Mag.*, vol. 22, no. 4, pp. 54–69, Jul. 2005.

[3] S. Zhang, S. Gao, G. Wang, and Y. Li, "Robust NLOS error mitigation method for TOA-based localization via second-order cone relaxation," *IEEE Commun. Lett.*, vol. 19, no. 12, pp. 2210–2213, Dec. 2015.

[4] Y. Zou and Q. Wan, "Asynchronous time-of-arrival-based source localization with sensor position uncertainties," *IEEE Commun. Lett.*, vol. 20, no. 9, pp. 1860–1863, Sep. 2016.

[5] K. Kowalczyk, E. A. P. Habets, W. Kellermann, and P. A. Naylor, "Blind system identification using sparse learning for TDOA estimation of room reflections," *IEEE Signal Process. Lett.*, vol. 20, no. 7, pp. 653–656, Jul. 2013.

[6] G. Wang and K. C. Ho, "Convex relaxation methods for unified near-field and far-field TDOA-based localization," *IEEE Trans. Wireless Commun.*, vol. 18, no. 4, pp. 2346–2360, Mar. 2019.

[7] R. M. Vaghefi and R. M. Buehrer, "Received signal strength-based sensor localization in spatially correlated shadowing," in *Proc. IEEE Int. Conf. Acoust., Speech Signal Process.*, Vancouver, BC, Canada, May 2013, pp. 4076–4080.

[8] P. Zuo, T. Peng, K. You, W. Guo, and W. Wang, "RSS-based localization of multiple directional sources with unknown transmit powers and orientations," *IEEE Access*, vol. 7, pp. 88756–88767, 2019.

[9] W. Li, Z. Yuan, S. Yang, and W. Zhao, "Error analysis on RSS range-based localization based on general log-distance path loss model," in *Proc. IEEE MASS*, Chengdu, China, Oct. 2018, pp. 469–474.

[10] R. Sari and H. Zayyani, "RSS localization using unknown statistical path loss exponent model," *IEEE Commun. Lett.*, vol. 22, no. 9, pp. 1830–1833, Sep. 2018.

[11] B. Zhang, H. Wang, T. Xu, L. Zheng, and Q. Yang, "Received signal strength-based underwater acoustic localization considering stratification effect," in *Proc. OCEANS*, Shanghai, China, Apr. 2016, pp. 1–8.

[12] M. R. Gholami, R. M. Vaghefi, and E. G. Ström, "RSS-based sensor localization in the presence of unknown channel parameters," *IEEE Trans. Signal Process.*, vol. 61, no. 15, pp. 3752–3759, Aug. 2013.

[13] Y. Wang and K. C. Ho, "Unified near-field and far-field localization for AOA and hybrid AOA-TDOA positionings," *IEEE Trans. Wireless Commun.*, vol. 17, no. 2, pp. 1242–1254, Feb. 2018.

[14] Y. Wang, K. C. Ho, and G. Wang, "A unified estimator for source positioning and DOA estimation using AOA," in *Proc. ICASSP*, Calgary, AB, Canada, Apr. 2018, pp. 3201–3205.

[15] A. Achroufene, Y. Amirat, and A. Chibani, "RSS-based indoor localization using belief function theory," *IEEE Trans. Autom. Sci. Eng.*, vol. 16, no. 3, pp. 1163–1180, Jul. 2019.
[16] S. Chang, Y. Li, W. Hu, H. Wang, and Y. Hu, "RSS-based target localization via semi-definite programming relaxation," in *Proc. IEEE APCC*, Ningbo, China, Nov. 2018, pp. 525–529.
[17] G. Wang, H. Chen, Y. Li, and M. Jin, "On received-signal-strength based localization with unknown transmit power and path loss exponent," *IEEE Wireless Commun. Lett.*, vol. 1, no. 5, pp. 536–539, Oct. 2012.
[18] K. Yu, "3-D localization error analysis in wireless networks," *IEEE Trans. Wireless Commun.*, vol. 6, no. 10, pp. 3473–3481, Oct. 2007.
[19] F. K. W. Chan, H. C. So, and W.-K. Ma, "A novel subspace approach for cooperative localization in wireless sensor networks using range measurements," *IEEE Trans. Signal Process.*, vol. 57, no. 1, pp. 260–269, Jan. 2009.
[20] S. Chang, Y. Li, H. Wang, W. Hu, and Y. Wu, "RSS-based cooperative localization in wireless sensor networks via second-order cone relaxation," *IEEE Access*, vol. 6, pp. 54097–54105, 2018.
[21] Z. Wang, H. Zhao, T. Lu, and T. A. Gulliver, "Cooperative RSS-based localization in wireless sensor networks using relative error estimation and semidefinite programming," *IEEE Trans. Veh. Technol.*, vol. 68, no. 1, pp. 483–497, Jan. 2019.
[22] S. Tomic, M. Beko, R. Dinis, and L. Berbakov, "Cooperative localization in wireless sensor networks using combined measurements," in *Proc. TELFOR*, Belgrade, Serbia, Nov. 2015, pp. 488–491.
[23] S. Tomic, M. Beko, and R. Dinis, "RSS-based localization in wireless sensor networks using convex relaxation: Noncooperative and cooperative schemes," *IEEE Trans. Veh. Technol.*, vol. 64, no. 5, pp. 2037–2050, May 2015.
[24] R. W. Ouyang, A. K.-S. Wong, and C.-T. Lea, "Received signal strength-based wireless localization via semidefinite programming: Noncooperative and cooperative schemes," *IEEE Trans. Veh. Technol.*, vol. 50, no. 3, pp. 1307–1318, Mar. 2010.
[25] G. Wang and K. Yang, "A new approach to sensor node localization using RSS measurements in wireless sensor networks," *IEEE Trans. Wireless Commun.*, vol. 10, no. 5, pp. 1389–1395, May 2011.
[26] S. Boyd and L. Vandenberghe, *Convex Optimization* Cambridge, U.K.: Cambridge Univ. Press, 2004.
[27] M. Grant and S. Boyd. *CVX: Matlab Software for Disciplined Convex Programming Version 1.21*. Accessed: Apr. 15, 2010. [Online]. Available: http://cvxr.com/cvx
[28] J. F. Sturm, "Using SeDuMi 1.02, a MATLAB toolbox for optimization over symmetric cones," *Optim. Methods Softw.*, vol. 11, nos. 1–4, pp. 625–653, 1999.
[29] K.-C. Toh, M. J. Todd, and R. H. Tütüncü, "On the implementation and usage of $SDPT_3$—A Matlab software package for semidefinite-quadratic-linear programming, version 4.0," in *Handbook Semidefinite, Conic Polynomial Optimization*, vol. 166. New York, NY, USA: Springer, 2011, pp. 715–754.
[30] J. C. Giacomin, L. H. A. Correia, T. Heimfarth, G. M. Pereira, V. F. Silva, and J. L. P. De Santana, "Radio channel model of wireless sensor networks operating in 2.4 GHz ISM band," *INFOCOMP J. Comput. Sci.*, vol. 9, no. 1, pp. 98–106, Oct. 2010.
[31] S. Willis and C. J. Kikkert, "Radio propagation model for long-range wireless sensor networks," in *Proc. 6th Int. Conf. Inf., Commun. Signal Process.*, Singapore, Dec. 2007, pp. 1–5.
[32] D. Li and H. Hu, "Least square solutions of energy based acoustic source localization problems," in *Proc. ICPPW*, Montreal, QC, Canada, Aug. 2004, pp. 443–446.
[33] I. Pólik and T. Terlaky, "Interior point methods for nonlinear optimization," in *Nonlinear Optimization*, G. Di Pillo and F. Schoen, Eds., 1st ed. Berlin, Germany: Springer-Verlag, 2010.
[34] S. Tomic, M. Beko, and R. Dinis, "3-D target localization in wireless sensor networks using RSS and AoA measurements," *IEEE Trans. Veh. Technol.*, vol. 66, no. 4, pp. 3197–3210, Apr. 2017.
[35] S. Tomic, M. Beko, R. Dinis, and P. Montezuma, "A closed-form solution for RSS-AOA target localization by spherical coordinates conversion," *IEEE Wireless Commun. Lett.*, vol. 5, no. 6, pp. 680–683, Dec. 2016.
[36] S. M. Kay, *Fundamentals Statistical Signal Processing: Estimation Theory*. Upper Saddle River, NJ, USA: Prentice-Hall, 1993.

QINKE QI received the B.S. degree in communications engineering from the Ningbo Institute of Technology, Zhejiang University, Ningbo, China, in 2018. He is currently pursuing the M.S. degree with the Faculty of Electrical Engineering and Computer Science, Ningbo University, Ningbo. His current research interest includes wireless localization.

YOUMING LI received the B.S. degree in computational mathematics from Lanzhou University, China, in 1985, the M.S. degree in computational mathematics from Xi'an Jiaotong University, Xi'an, China, in 1988, and the Ph.D. degree in electrical engineering from Xidian University, Xi'an, in 1995.

From 1988 to 1998, he was an Associate Professor with the Department of Applied Mathematics, Xidian University. From 1999 to 2004, he was with the School of Electrical and Electronics Engineering, Nanyang Technological University, DSO National Laboratories, Singapore, and the School of Engineering, Bar-Ilan University, Israel. Since 2005, he has been with Ningbo University, Ningbo, China, where he is currently a Professor. His research interests include cognitive radio and wireless/wireline communications.

YONGQING WU received the B.S. degree in communications engineering from Xidian University, Xi'an, China, in 1990, the M.S. degree in computer science and technology from the Hebei University of Technology, Tianjin, China, in 1998, and the Ph.D. degree in measurement technology and instruments from Tianjin University, Tianjin, in 2001.

From 1990 to 1995, he was a Technical Development Manager with the Department of Technical Development, Tianjin Land Sea Technology Company Ltd. Since 2001, he has been with the Institute of Acoustics, Chinese Academy of Sciences, Beijing, China, where he is currently a Professor. His research interests include detection and recognition of underwater target and underwater acoustic positioning and navigation.

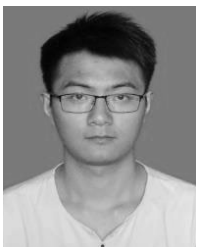

YONG WANG received the B.S. degree in communications engineering from the City Institute, Dalian University of Technology, Dalian, China, in 2017. He is currently pursuing the M.S. degree with the Faculty of Electrical Engineering and Computer Science, Ningbo University, Ningbo, China. His current research interest includes pulse interference in power line communication systems.

YIN YUE received the B.S. degree in electronic information engineering from the Huzhou Teachers College, Huzhou, China, in 2017. She is currently pursuing the M.S. degree with the Faculty of Electrical Engineering and Computer Science, Ningbo University, Ningbo, China. Her current research interest includes spectrum sensing.

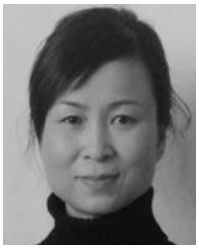

XUPENG WANG received the degree in digital communication from Xidian University. She is currently an Engineer with Information Center, Ningbo University. Her research interests include wireless communication with applications.